Scintillation Distance Measurements

Siqi Liu[1,3]⋆, Ue-Li Pen[1,2]†, J-P Macquart[4]‡, Walter Brisken[5]§, Adam Deller[6]¶

[1] *Canadian Institute for Theoretical Astrophysics, University of Toronto, M5S 3H8 Ontario, Canada*
[2] *Canadian Institute for Advanced Research, Program in Cosmology and Gravitation*
[3] *Department of Astronomy and Astrophysics, University of Toronto, M5S 3H4, Ontario, Canada*
[4] *ICRAR-Curtin University of Technology, Department of Imaging and Applied Physics, GPO Box U1978, Perth, Western Australia 6102, USA*
[5] *National Radio Astronomy Observatory, P.O. Box O, Socorro, NM 87801, USA*
[6] *ASTRON, the Netherlands Institute for Radio Astronomy, Postbus 2, 7990 AA, Dwingeloo, The Netherlands*

23 April 2015

ABSTRACT
We show how interstellar scintillations, combined with VLBI measurements, can be used to measure distances. We apply the technique to archival data on PSR B0834+06, concluding that for this example the plasma lenses can be precisely modelled using the (Pen & Levin 2014) inclined sheet model, resulting in two distinct lens planes. This data strongly favours the reconnection sheet model over turbulence as the primary source of pulsar scattering. A global conformal distance degeneracy exists which allows a rescaling of the absolute distance scale. This degeneracy is broken if the pulsar resides in a binary system, which is the case for most precision timing targets.

Key words: Pulsar

1 INTRODUCTION

Pulsars have long provided a rich source of astrophysical information due to their compact emission and predictable timing. One of the weakest measurements for most pulsars is their direct geometric distance. For some pulsars, timing parallax or VLBI parallax has resulted in direct distance determinations. For most pulsars, the distance is a major uncertainty for precision timing interpretations, including mass, moment of inertia, and gravitational wave direction (Boyle & Pen 2012).

Direct VLBI observation of PSR B0834+06 shows multiple images lensed by the interstellar plasma. Combining the angular positions and scintillation delays, the authors published the derived effective distance (Brisken et al. 2010) of approximately 1168 ± 23 pc for apexes whose time delays range from 0.1 ms to 0.4 ms, and 1121 ± 59 pc for 1 ms apexes. This represents a precise measurement compared to all other attempts to derive distances to this pulsar. This effective distance is a combination of pulsar-screen and earth-screen distances, and does not allow a separate determination of the individual distances. A binary pulsar system would in principle allow a breaking of this degeneracy (Pen & Levin 2014). One potential limitation is the precision to

which the lensing model can be understood. In this paper, we demonstrate that the lensing screen consists of nearly parallel linear refractive structures, in two screens. The precise model confirms the one dimensional nature, and thus the small number of parameters that need to be measured to quantify the lensing screen.

2 LENSING

2.1 B0834+06

Our analysis is based on the reduced apex catalog from (Brisken et al. 2010). Information from each identified apex includes delay τ, delay rate (differential frequency f_D), Right Ascension α, declination δ, error of α σ_α and error of δ σ_δ. Data of each apex are collected from four dual circular polarization 8 MHz wide sub-bands spanning the frequency range $310.5 - 342.5$ MHz.

We divide the apex data into two groups according to the time delay, one group ranges from 0.1 ms to 0.4 ms and the other group has time delay at about 1 ms. The statistics of the positions of the points are: for 0.4 ms group, there are 10 apexes in the first two sub-bands, and 14 apexes in the last two sub-bands; for 1 ms group, there are 5 apexes in the first sub-band, 6 apexes in the second sub-band, 5 apexes in the third sub-band, and 4 apexes in the last sub-band.

To match the same apexes in different sub-bands, we convert the differential frequency in different sub-bands to the one in 322.5 MHz, by $f_D/f_{\text{band}} \cdot 322.5$ MHz. Then we

⋆ E-mail: sqliu@cita.utoronto.ca
† E-mail: pen@cita.utoronto.ca
‡ E-mail:J.Macquart@curtin.edu.au
§ Email:wbrisken@aoc.nrao.edu
¶ E-mail:deller@astron.nl

map a total of 9 apexes from the 0.4 ms group, and 5 apexes from the 1 ms group. This results in an estimation for the average value in $f = 322.5$ MHz and standard deviation among four sub-bands. They are listed in Table 1. The f_D and τ are the arithmetic mean value of the four sub-bands $\bar{x} = \sum_{i=1}^{n=4} x_i/4$, x is for f_D or τ. The mean value of α and δ are the weighted mean, calculated by following equation:

$$x = \sum_{i=1}^{n=4} \frac{x_i}{\sigma_i{}^2},$$

Here x is for α or δ. The angle of the scintillation image away from the pulsar is defined as $\theta^2 = \alpha^2 + \delta^2$.

The method we use to calculate the error of time delay τ or differential frequency f_D is by following equation:

$$\sigma_{\tau, f_D}^2 = \frac{\sum_{i=1}^{n=4} (x_i - \bar{x})^2}{4 \cdot 3},$$

and $i = 4$ because there are four sub-bands. This is also how we calculate the sample error of α and δ, marked with errorbars in Figure 3.

The way we use to calculate the population error of α and δ, which is the σ_α and σ_δ listed in Table 1, is defined by following equation:

$$\left(\frac{1}{\sigma_{\alpha,\delta}}\right)^2 = \sum_{i=1}^{n} \frac{1}{\sigma_i{}^2},$$

where i ranges from 1 to 4, for four sub-bands, and σ_i is the error of the data in each sub-band. They are marked with circles in Figure 3.

2.2 Solution in one lens model

2.2.1 Distance of the lens

In the absence of a lens model, the fringe rate, delay and angular position cannot be uniquely related. To interpret the data, we adopt the lensing model of (Pen & Levin 2014). In this model, the lensing is due to projected fold caustics of a thin sheet closely aligned to the line of sight.

How distance of the pulsar is related to the time delay τ and angle θ, and how velocity is related to the differential frequency f_D are defined by the following equations:

$$\tau = \frac{D_e \theta^2}{2c},$$

$$f_D = f \cdot \frac{d\tau}{dt},$$

where D_e is the effective distance. If we name the distance of the pulsar D_{po}, the distance of the lens D_{so}, the effective distance is equivalent to the distance of the lens placed at the middle point of the pulsar: $D_e = D_{po}D_{so}/(D_{po} - D_{so})$.

We make a plot describing the relation of $\theta - \sqrt{\tau}$ in Figure 2. A least square effective distance results in $D_e^1 = 1017.1 \pm 2.8$ for the 0.4 ms apexes on lens 1 and $D_e^2 = 1243 \pm 64$ for the 1 ms apexes on lens 2. This indicates that the lens 1 is closer to the pulsar.

Take $D_e^1 = 1017.1$ pc, combined with the VLBI measured distance of the pulsar 640 pc, the distance of lens 1 D_{1o}, where 0.4 ms scintillation points are refracted, is equal to 392.8 pc. For 1 ms apexes, the distance of lens 2 is equal to

422.5 pc. Thus, the degeneracy of the distance of the screen is broken.

2.2.2 Angular position of 0.4 ms points

We fit a line to the observed angular positions of the 0.4 ms group, which has an positive angle of $\gamma = -25.2°$ (east of the declination axis). We use this axis to define $\theta_\parallel$ and define $\theta_\perp$ by a 90° clockwise rotation from it.

We calculate θ from the $\theta - \sqrt{\tau}$ relation and observed τ. Then the angular positions of the 0.4 ms group are calculated:

$$\alpha = -\theta \cdot \sin\gamma,$$

$$\delta = -\theta \cdot \cos\gamma.$$

They are marked out with the scatter points on the left side in Figure 3.

2.2.3 Angular positions of 1 ms group

We calculate the positions of the 1 ms apexes in following steps. First, matching the θ-τ relation, which is plotted in Figure 2, we calculate the θ from observation τ. Note that we define the velocity that is in the direction of the pulsar. Second, we consider the point with the largest θ among this 1 ms group, named 5, share the same $\theta_\parallel$ with the point with the largest θ among the 0.4 ms group, named 6. $\theta_\perp$ is calculated by $\theta_\perp = \sqrt{\theta^2 - \theta_\parallel^2}$. Then, by using a rotation matrix defined by γ, the position of point 5 is determined: $(-10.78, -24.35)$ mas.

Third, to determine the position of the rest points $1-4$, we need to know the velocity of the pulsar, and then fit the α and δ to get the same differential frequency with the observation. To know the velocity of the pulsar, we calculated the velocity component in two directions: $v_\parallel$ according to the differential frequency of point 6 in 0.4 ms group and $v_\perp$, the parallel direction is defined by the the axis that is γ away from declination axis. v_{A5} (in the direction pointing from point 5 to A), which has the component in the transverse direction of the velocity can be calculated withe the differential frequency of point 5. More specifically, in a time period of 6500 s (dt = 6500 s), we will solve two equations:

$$d\tau = \tau(t = 0s) - \tau(t = 6500 \text{ s}, v_\parallel) \quad = f_{D6}/f \cdot dt,$$
$$d\tau = \tau(t = 0s) - \tau(t = 6500 \text{ s}, v_{A5}) \quad = f_{D5}/f \cdot dt,$$

where $f = 322.5$ MHz. Then we know the $v_\perp$ component by v_{A5}, and furthermore, the total velocity of the pulsar v_{tot} and its angle to the north axis ϵ, note that the east direction is the positive direction. The result is $v_\parallel = 180.3$ km/s and $v_{A5} = 159.6$ km/s. Thus the total velocity is 188.5 km/s and with $\epsilon = -8.25°$ away from the declination axis.
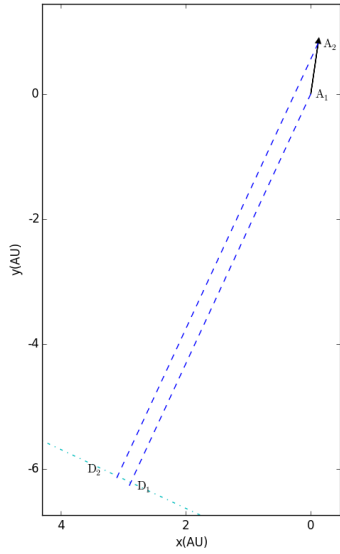
The example of how the lensed image changes with the moving of the pulsar is plotted in Figure 1.

Fourth, we fit the position of the rest four points, with known proper motion of the pulsar. For example, point 4:

$$\tau(t = 0s) - \tau(t = 6500 \text{ s}, v_{A4}) = f_{D4}/f \cdot dt,$$
$$v_{tot} \cdot \sin)(\tan^{-1}(\alpha, \delta)) - \gamma] = v_{A4},$$
$$\alpha^2 + \delta^2 = \theta^2$$

Figure 1. The moving of the lensed image with the moving of the pulsar. x axis and y axis are the relative distance to the position of the pulsar. A_1 is the original position of the pulsar, and A_2 is the position of the pulsar after 650000s (7.5 days). Dash line is the line of the incoming light. Dot dash line is the place where lensed image on lens 1 lies. D_2 is the place where the lensed image lie when the pulsar moved to A_2.

We fit a line to this five calculated points, to describe these the positions of these 5 points.

The time in last column of Table 1 is calculated with $2\tau f/f_D$, equivalent to pulsar moving at 640 pc plane from the original position to the lensed image position with the calculated velocity of the pulsar in that direction in one lens model.

That is one lens model fitting. Knowing time delay τ, we can get the distance of the screen; knowing the position of point 5 and the differential frequency f_D, we can get the velocity of the pulsar; knowing the velocity and observation diffferential frequency, we can get the position of points $1-4$.

2.3 Discussion of one lens model

The 0.4 ms group lens solution appears consistent with the premise of the inclined sheet lensing model (Pen & Levin 2014).

For 1 ms group, lens 2 only images a subset of the lens 1 images. This could happen if lens 1 screen is just under the critical inclination angle, such that only $3-\sigma$ waves lead to a fold caustic. If the lens 2 was at a critical angle, the chance of encountering a somewhat less inclined system is of order unity. More surprising is the absence of a single refraction image of the pulsar, which is expected at position J. This could happen if the maximum refraction angle is just below critical, such that only rays on the appropriately aligned double refraction can form images. This scenario predicts that at frequencies just below 300 MHz, or a few weeks earlier in time, the pulsar should be seen at position J. We made a plot of the refraction angle β in the direction that is

transverse to the first lens plane in Figure 6. From our calculation, it takes 22 days for the puslar to move from point 1 on lens 1 to J, and it takes 44 days for the pulsar to move from point 5 on lens 1 to J. The data spans about 10% in frequency, making it unlikely that single lens image J would not be seen due to the larger required refraction angle. Instead, we speculate that the fold caustic could have formed near double lens image 1, and thus only intersections with the closer lens plane caustic south of image 1 are double lensed.

2.4 Double lens model

2.4.1 Solving the double lens model

We name the position of the pulsar point A, position of the lensed image on lens 2 point H, position of the lensed image on lens 1 point B, position of the observer point O, pedal from the pulsar to line HJ point J, the pedal from point H to line BD point F, and the pedal from point B to line HJ point G, for easier discussion. Because points $1-4$ share the approximately same time delay with point 5, the lens where the image formed should be at the same distance away from us. The only reasonable position of screen (line HJ) that fits all these five points, marked with a solid line in Figure 3. That is unrealistic for the structure of the interstellar medium.

Therefore, we consider another model candidate: the double lens model. Respective calculation shows that the light is first refracted by the lens 2 and then refracted by lens 1.

The first step is to calculate the position of J. We make an estimate of the distance of J by the 1 ms $\theta - \tau$ relation, and then we calculated the position of J by matching the time delay of point 2 and point 5. The result shows that lens 2 is 425 pc away from us. And its position is marked in Figure 3. Because J is the pedal to lens 2, we made a line that is perpendicular to AJ, the solid line in Figure 3. This is lens 2.

The second step is to find the matched pairs of those two lenses. By try and error, we found that the 5 points in 0.4 ms group that have the largest θ should be the candidates where lens 1 lie. These five matched lines are marked with dot dash lines in Figure 3 and their values are listed in the first two columns in Table 2. They are the located at a distance 392.8 pc away from us. Here we define three distances:

$$D_{p2} = 640 \text{ pc} - 425.0 \text{ pc} = 215.0 \text{ pc},$$
$$D_{12} = 425 \text{ pc} - 392.8 \text{ pc} = 32.2 \text{ pc},$$
$$D_{1O} = 392.8 \text{ pc} - 0 \text{ pc} = 392.8 \text{ pc},$$

where D_{p2} is the distance from the pulsar to lens 2, D_{12} is the distance from lens 2 to lens 1, and D_{1O} is the distance from lens 1 to the observer.

Figure 4 and Figure 5 are examples of how light are being refracted on the first lens plane and the second lens plane. We specifically chose the point with $\theta_{1\parallel}$ equal to -17.44 mas on lens 1 for instance. We solve the solutions in

double lens model by following equations:

$$\frac{\text{JH}}{D_{p2}} = \frac{\text{HG}}{D_{12}},$$

$$\frac{\text{FB}}{D_{12}} = \frac{\text{BD}}{D_{1O}}.$$

The solved positions are plotted in Figure 3, and respective time delays and differential frequencies are listed in Table 2. For the error of time delay τ, we just use the following equation:

$$\left(\frac{\sigma_{\text{tot}}}{\tau_2}\right)^2 = \left(\frac{\sigma_{\tau1}}{\tau_1}\right)^2 + \left(\frac{\sigma_{\tau2}}{\tau_2}\right)^2,$$

where $\sigma_{\tau1}$ represents the sample error from the 0.4 ms group on lens 1, and $\sigma_{\tau2}$ represents the sample error from respective 1 ms group on lens 2, τ_1 is the time delay from 0.4 ms group, and τ_2 is the time delay from respective 1 ms group.

2.4.2 *Comparing calculated result in double lens model and observation data*

Comparing τ, we time delay for these five points, and list the results in Table 2. For point 2 and 5, they fit perfectly because these are the two points that we use these to calculate the position of J; for the rest three points, all of the calculated results are still within $3 - \sigma$ region of the observation time delays.

To compare differential frequency f_D, we need to calculate the velocity of the pulsar and the velocity of the lens. We consider lens 1 to be relative static, both the velocity of the pulsar and the velocity of lens 2 mentioned later are the relative velocities to lens 1. To calculate the velocity of the pulsar, we need two components, the $v_\parallel$ in $\theta_\parallel$ direction, and $v_\perp$ in $\theta_\perp$ direction. For $v_\parallel$, we still use the velocity that is calculated in 0.4 ms group in one lens model, that is 180.3 km/s. For the velocity of lens 2, because it is a line, and we do not consider radial velocity, so it could only be in the direction of AJ. However, by calculation, the $\angle$DAH is 98° by calculation, that means $v_\perp$ and v_{lens2} are nearly degenerate. In the following discussion, we consider lens 2 to be static and only take $v_\perp$ into account.

To calculate $v_\perp$, we choose the point 2, which has the smallest errorbar of differential frequency. In a time period of 6500 s, we solved that the $v_\perp$ should be 7.3 km/s, in the direction pointing from B to D, to make the calculated f_{D2} match the observation f_D. Thus the v_{tot} is solved to be 192.6 km/s, with an angle $\epsilon = 4.59°$ west of north, which is marked on the top of the star in Figure 3.

With this velocity of the pulsar, we calculate the differential frequency of point 1,3,4 and 5. Results are listed in Table 2. The calculated results all lie in the $3 - \sigma$ region of the observation data.

3 POSSIBLE IMPROVEMENTS

We discuss several strategies which can improve on the solution accuracy. The single biggest improvement would be to monitor over a week, when the pulsar crosses each individual lens, including both lensing systems.

Angular resolution can be improved using longer baselines, for example adding a GMRT-GBT baseline doubles the resolution. Observing at multiple frequencies over a
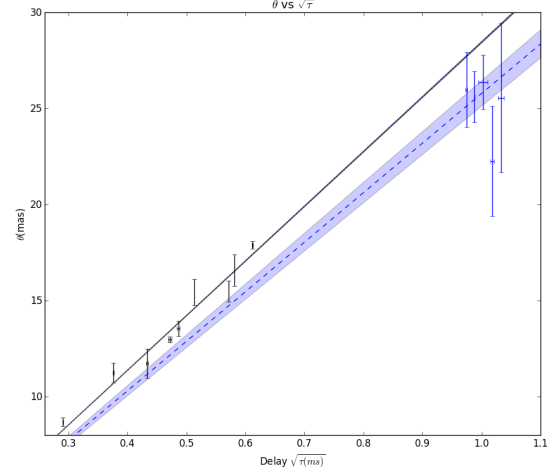

Figure 2. θ vs $\sqrt{\tau}$. Two separate lines through the origin were fitted to the points sampled among the 0.4 ms group and 1 ms group. The solid line is the fitted line of the 0.4ms positions, where $k = 28.51$ with an error region of $\sigma_k = 0.04$. The dashed lines are the fitted lines of the 1ms position, where $k = 25.78$ with an error region of $\sigma_k = 0.66$.
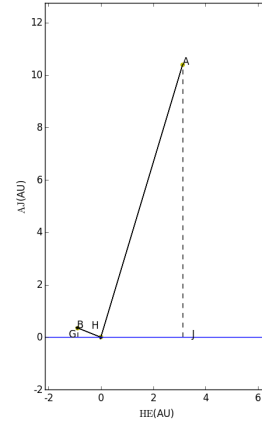
Figure 4. Refraction on lens 2. A is the position of the pulsar. H is the lensed image on lens 2. B is the lensed image on lens 1. J is the pedal of A to lens 2, and G is the pedal of B to lens 2. v_{JH} and v_{HG} should be equal, which is described in Section 2.4. In this case, $\theta_{1\parallel} = -17.44$ mas.

longer period allows for a more precise measurement: when the pulsar is between two lenses, the refraction angle β is small, and one expects to see the lensing at higher frequency, where the resolution is higher, and distances between lenses positions can be measured to much higher accuracy.

Holographic techniques (Walker et al. 2008; Pen et al. 2014) may be able to measure delays, fringe rates, and VLBI positions substantially more accurately. Combining these techniques, the interstellar lensing could conceivably achieve distance measurements an order of magnitude better than the current published effective distance errors. This could bring most pulsar timing array targets into the coherent tim-
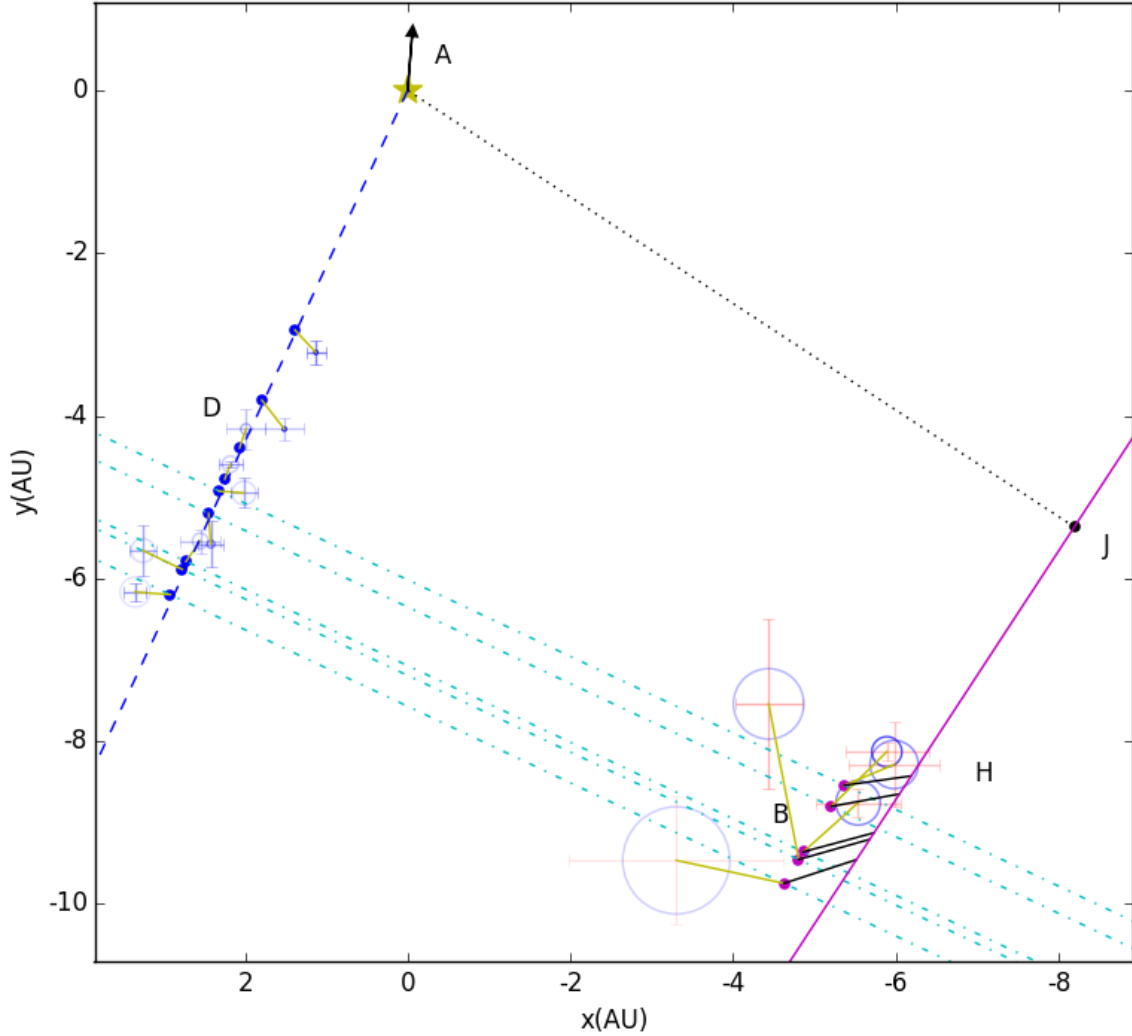
Figure 3. Observed and calculated angular positions of 0.4 ms and 1 ms data in double lens model. x axis and y axis are the relative distance to the position of the pulsar in Right Ascension direction and declination direction, on a 2D plane that is transverse to the line of sight. The position of the screen locate at 392.8 pc and 425.0 pc respectively. Scatter points on the left side, marked with letter D, are the calculated positions from the 0.4 ms apexes observation. Dash line is the fitted line of 0.4 ms apexes positions, with a angle $\gamma = -25.2°$ east of north. The points lie on the left side with errorbars, are the observation points with their sample errors; while the circles are plotted with population errors. Short solid lines between them are the matched positions of the observation positions and the calculated positions. The scatter points on the right side, marked with letter B, are the calculated lensed image on lens 1 from 1 ms group. The short solid line connects the lensed image one lens 1(observable) and lensed image 2(unobservable), marked with letter H. Long solid line is the fitted line of these positions. Those points with errorbars nearby are the observation points with their sample errors, while the circles are plotted with population errors. The dotted line on the top right side is vertical to the solid line, and the pedal is called J. Short light solid lines connect the observation points and the calculated positions in 1 ms group. Middle dot dash lines connect the 0.4 ms and 1 ms calculated positions with the same $\theta_{1\parallel}$, which are lens 1. The proper motion of the pulsar is 192.6 km/s, with an angle $\epsilon = -4.59°$ east of north, is marked with an arrow from the star, point A the position of the pulsar, at the top of the figure.

| $\theta_{1\parallel}$(mas)	f_D(mHz)	σ_{f_D}(mHz)	τ_1(ms)	$\sigma_{\tau 1}$(ms)	α(mas)	σ_α(mas)	δ(mas)	σ_δ(mas)	time(day)
-8.29	-12.94	0.19	0.0845	0.0005	2.87	0.11	-8.201	0.088	49.9
-10.71	-16.80	0.28	0.14123	0.0009	3.86	0.07	-10.563	0.053	64.5
-12.36	-18.92	0.23	0.188	0.002	5.06	0.20	-10.58	0.13	74.4
-13.44	-20.40	0.49	0.222	0.003	5.55	0.30	-11.73	0.21	80.8
-13.86	-21.17	0.61	0.236	0.002	5.12	0.43	-12.56	0.31	83.4
-14.63	-22.32	0.47	0.2633	0.0003	6.16	0.14	-14.15	0.10	88.0
-16.29	-24.63	0.40	0.327	0.003	6.49	0.29	-14.06	0.20	98.0
-16.57	-24.94	0.44	0.338	0.0003	8.29	0.42	-14.37	0.32	99.7
-17.44	-26.09	0.36	0.3743	0.0006	8.53	0.52	-15.74	0.42	105
$\cdots$	-35.06	0.52	0.9495	0.0016	-15.23	0.69	-21.06	0.70	202
$\cdots$	-38.31	0.64	0.97633	0.00088	-15.02	0.48	-20.74	0.38	190
$\cdots$	-40.17	0.55	1.0045	0.0079	-14.14	0.66	-22.27	0.62	187
$\cdots$	-41.27	0.54	1.0370	0.0032	-11.28	0.93	-19.2	1.1	188
$\cdots$	-43.08	0.44	1.0663	0.0050	-8.4	1.7	-24.1	1.4	185

Table 1. 0.4 ms and 1 ms observation data and calculated data. The upper part of the table list the 0.4 ms group data, while the 1 ms group lie in the lower part of the table. Observation data include the differential frequency f_D, time delay τ from scintillation measurement (τ_1 for 1 ms data and τ_2 for 0.4 ms data); α and δ from the VLBI measurement. The method of how to calculate the error of time delay, differential frequency and the last column time is mentioned in Section 2.1.

Lens 1 $\theta_{1\parallel}$ (mas)	Lens 2 $\theta_{2\parallel}$(mas)	τ_2(ms)	σ_{tot}(ms)	Calculated τ(ms)	f_D(mHz)	σ_{f_D}(mHz)	Calculated f_D(mHz)
-13.86	-12.71	0.9495	0.0095	0.955	-35.1	1.3	-37.22
-14.63	-14.69	0.9763*	0.0015	0.9763	-38.3†	1.0	-38.31
-16.29	-15.78	1.005	0.011	1.0272	-40.17	0.86	-40.64
-16.57	-16.35	1.0370	0.0033	1.036	-41.27	0.90	-41.04
-17.44	-17.44	1.0663*	0.0052	1.066	-43.08	0.74	-42.26

Table 2. Comparison of time delay τ and the differential frequency f_D of the observation data and the calculated result in double lens model. $\theta_{1\parallel}$ is the angle of the 0.4 ms group with the component in the axis defined by γ. $\theta_{2\parallel}$ is the angle of the 1 ms group with the component in the axis defined by γ. The values with star symbols on them are the points that we use to calculate the position of J and the point with a † symbol is the point that we use to calculate the velocity of the pulsar v_{A2}.
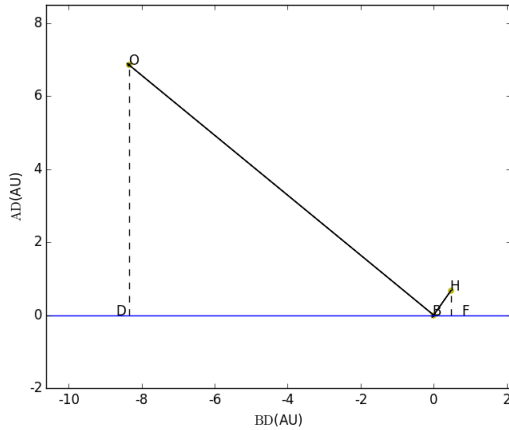
Figure 5. Refraction on lens 1. H is the lensed image on lens 2. B is the lensed image on lens 1. O is the position of the observer. F is the pedal of H to lens 2, and D is the pedal of O to lens 2. v_{FB} and v_{BD} should be equal, which is described in Section 2.4. In this case, $\theta_{1\parallel} = -17.44$ mas.
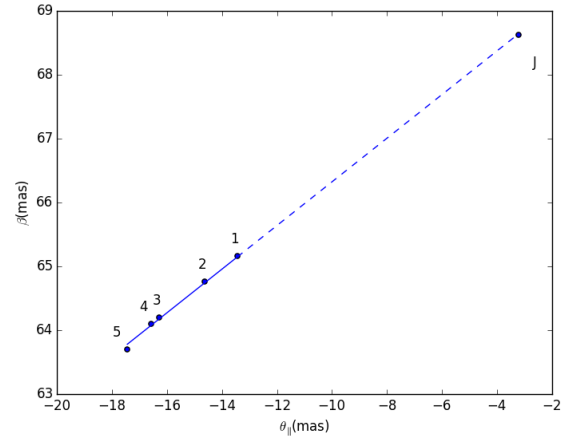
Figure 6. (π-$\angle$AHB) vs $\theta_{1\parallel}$. β_J is calculated with J as the lensed image on lens 2, and $\theta_{1\parallel} = -3.21$ mas.

ing regime, enabling arc minute localization of gravitational wave sources, lifting any potential source confusion.

Ultimately, the precision of the lensing results would be limited by the fidelity of the lensing model. In the in-

clined sheet model, the images move along fold caustics. The straightness of these caustics depends on the inclination angle, which in turn depends on the amplitude of the surface waves.

4 CONCLUSIONS

We have applied the (Pen & Levin 2014) inclined sheet model to archival apex data of PSR B0834+06. The data is well fit by two linear lensing screens, with nearly plane-parallel geometry. This appears a natural consequence of very smooth reconnection sheets, and are an unlikely outcome of ISM turbulence. These results, if extrapolated to multi-epoch observations of binary systems, this might result in accurate distance determinations.

5 ACKNOWLEDGEMENTS

REFERENCES

Boyle L., Pen U.-L., 2012, Phys. Rev. D, 86, 124028

Brisken W. F., Macquart J.-P., Gao J. J., Rickett B. J., Coles W. A., Deller A. T., Tingay S. J., West C. J., 2010, ApJ, 708, 232

Pen U.-L., Levin Y., 2014, MNRAS, 442, 3338

Pen U.-L., Macquart J.-P., Deller A. T., Brisken W., 2014, MNRAS, 440, L36

Walker M. A., Koopmans L. V. E., Stinebring D. R., van Straten W., 2008, MNRAS, 388, 1214